


**Dissipation-driven quantum phase transitions and symmetry breaking**

Julia Hannukainen and Jonas Larson

*Department of Physics, Stockholm University, Se-106 91 Stockholm, Sweden* (Received 26 April 2017; revised manuscript received 22 September 2017; published 15 October 2018)

By considering a solvable driven-dissipative quantum model, we demonstrate that continuous phase transitions in dissipative systems may occur without an accompanying symmetry breaking. As such, the underlying mechanism for this type of transition is qualitatively different from that of continuous equilibrium phase transitions. In our model, the transition is solely a result of the interplay between Hamiltonian and dissipative dynamics and manifests as a nonanalyticity in the steady state  $\hat{\rho}_{ss}$  in the thermodynamic limit. Based on knowledge from critical classical models we suggest that this behavior derives from a rounding of a first-order phase transition into a continuous one due to large environment-induced fluctuations. Despite being conceptually different from the traditional continuous transitions, we show that expectations of local observables can still be characterized by a set of critical exponents.

DOI: [10.1103/PhysRevA.98.042113](https://doi.org/10.1103/PhysRevA.98.042113)**I. INTRODUCTION**

The concept of spontaneous symmetry breaking [1] plays a central role in physics, ranging from classical thermodynamics to the standard model of high-energy physics. In the Landau theory of equilibrium phase transitions [2], the symmetry-broken phase is characterized by a nonzero local order parameter, while the unordered phase is identified by a vanishing order parameter. This mean-field theory also predicts that the physics in the vicinity of the critical points is entirely described by a few critical exponents. Scale invariance and the renormalization group provide additional understanding of critical behavior and especially its universal properties; continuous phase transitions (second-order transitions) can be grouped into different universality classes where their properties depend only on macroscopic properties, i.e., dimensionality and symmetries [1]. However, with the discovery of topological phase transitions and Kosterlitz-Thouless transitions it was understood that not all continuous phase transitions are accompanied with a symmetry breaking or a local order parameter [1,3]. For classical systems, it has also been shown that fluctuations or disorder may “melt” a discontinuous first-order phase transition into a continuous one [4].

Recently one type of nonequilibrium phase transitions that occur in driven-dissipative quantum systems has especially gained much attention due to its relevance to well-controlled quantum optical experiments [5–7]. Here the nonanalyticity, characteristic of the phase transition, appears in the system’s nonequilibrium steady state (NESS)  $\hat{\rho}_{ss}$  rather than its ground state as for quantum phase transitions [8]. By tailoring the system-environment couplings and the driving, it is possible to prepare a desirable  $\hat{\rho}_{ss}$  [7] and, hence, also cause behaviors reminiscent of continuous phase transitions [5]. Naturally, compared to equilibrium phase transitions very little is known about this new nonequilibrium quantum critical behavior. Any coupling to an environment will inevitably introduce additional fluctuations which could alter the critical

exponents [9] and the properties of the phases [10]. In cases it may even prohibit the build-up of long-range order in the system [11]. One natural question arises whether fluctuations due to the surrounding environment may even change the type of transition, like for classical systems a first-order phase transition can become continuous by inclusion of fluctuations [4]. The situation becomes more delicate though when the phase transition itself results from the coupling to the environment, i.e., it stems from the interplay between unitary and dissipative dynamics [10,12,13]. In this scenario the state  $\hat{\rho}_{ss}$  can typically not be linked to phases of the Hamiltonian, and their properties may be very distinct from equilibrium states.

The present paper demonstrates that for driven-dissipative systems continuous phase transitions may occur without any symmetry breaking. The origin of the transition can be traced back to a first-order phase transition which turns continuous in the so-called “bad cavity limit.” In particular we consider a set of coherently driven two-level “atoms” coupled to a lossy photon mode. In a strict sense the model cannot be considered a many-body system, but nevertheless it still shows quantum properties. More precisely, this is a paradigm setting for optical bistability [14,15] and where the hysteresis marks the appearance of a first-order phase transition. In recent years, optical bistability has been put in the context of NESS phase transitions [16,17], and especially the role played by quantum fluctuations has been thoroughly explored [16]. Even though quantum fluctuations are not strong in our model, we provide insight into the bistability mechanism. By considering the bad cavity limit, and as the photon mode is adiabatically eliminated, one finds an effective model for the atoms with an analytically solvable steady-state solution. Importantly the bistability, which at the mean-field level is connected to a first-order phase transition, turns into a continuous transition. Thus, like for classical systems [4], our work shows how the nature of a phase transition can change also in quantum systems when fluctuations become extensive.

The paper is structured as follows. In the next section we first define what is meant with NESS criticality for quantum systems, and then we introduce our model. We give a derivation of the corresponding Lindblad master equation, which is helpful when understanding the origin of the phase transition. The results are presented in Sec. III. First, we demonstrate the criticality from a mean-field analysis, and then we switch to the full quantum problem. We show how a continuous phase transition can result even in a system lacking any symmetries, and we also discuss the quantum properties, like entanglement, in the vicinity of this type of critical point. Finally we conclude in Sec. IV.

## II. MODEL SYSTEM

### A. Dissipation-driven phase transitions

To date, engineered driven-dissipative systems are mainly found in the AMO (atomic, molecular, and optical) community, and especially within trapped ions [7] and cold atoms [18]. These experiments are well described by a Markovian-Lindblad master equation [19]

$$\begin{aligned} \frac{\partial}{\partial t} \hat{\rho} &= \hat{\mathcal{L}}[\hat{\rho}] \\ &= i[\hat{\rho}, \hat{H}] + \sum_i \gamma_i (2\hat{L}_i \hat{\rho} \hat{L}_i^\dagger - \hat{L}_i^\dagger \hat{L}_i \hat{\rho} - \hat{\rho} \hat{L}_i^\dagger \hat{L}_i), \end{aligned} \quad (1)$$

where we have defined the Liouvillian  $\hat{\mathcal{L}}$ . The first term on the right represents the unitary evolution generated by  $\hat{H}$  (system Hamiltonian plus Lamb shifts), while the second term incorporates the effects stemming from the coupling to the environment with the decay rates  $\gamma_i$  ( $\geq 0$ ) and “jump” operators  $\hat{L}_i$ .

Equilibrium quantum phase transitions can be attributed nonanalyticity to the ground state for some critical coupling  $g_c$  in the thermodynamic limit. For a dissipative system the ground state is replaced by the steady state  $\hat{\rho}_{ss}$  of Eq. (1), and a phase transition is again marked by a nonanalyticity emerging in the thermodynamic limit. As for the standard equilibrium classification of phase transitions, for a continuous (second-order) NESS phase transition the expectation values of local observables  $O = \text{Tr}[\hat{O}\hat{\rho}_{ss}]$  should be continuous but with possible discontinuous first-order derivatives.

For any Hermitian jump operators  $\hat{L}_i = \hat{L}_i^\dagger$ , the maximally mixed state  $\hat{\rho}_{ss} = \mathbb{I}/D$  with  $D$  the Hilbert space dimension is clearly a steady state. If further  $[\hat{H}, \hat{L}_i] = [\hat{L}_i, \hat{L}_j] = [\hat{L}_i, \hat{L}_j^\dagger] = 0 \forall i, j$  the steady states are diagonal in the energy eigenbasis, i.e.,  $\langle \varepsilon_n | \hat{\rho}_{ss} | \varepsilon_m \rangle = p_n \delta_{nm}$  for some weights  $p_n$  and with  $|\varepsilon_n\rangle$  the  $n$ th eigenstate of  $\hat{H}$ . In particular, the ground state  $|\varepsilon_0\rangle$  is a “dark state” that is transparent to the effect of the environment. Such a model describes dephasing in the energy basis, and criticality does not derive from environmental fluctuations. As an alternative to the above, criticality driven by the environment stems from noncommutability among  $\hat{H}$  and the jump operators [20]. In this scenario,  $\hat{\rho}_{ss}$  is not necessarily a simultaneous dark state of the jump operators and an eigenstate of the Hamiltonian. Regardless of the situation, the existence and especially the uniqueness of steady states of Lindblad master equations are relevant questions that have been explored [21]. It is only recently, however, that general

properties of  $\hat{\rho}_{ss}$  in terms of phase transitions and novel phases of matter have been explored.

### B. Derivation of the microscopic model

When understanding how a continuous phase transition, which is not supported by a symmetry breaking, may arise, it is insightful to go back to the full Hamiltonian system that incorporates the full system and its environment. Namely, we aim at tracing the origin of the transition in the full model and explore its character in that setting.

We have in mind a set of  $K$  two-level atoms that couple identically to a single-photon mode. The collective atomic dissipation is generated by photon losses to a zero temperature environment (an alternative system is considered in Ref. [22]). The full microscopic Hamiltonian is then decomposed into three subsystems and their interactions: the atoms, the cavity photon mode, and the environment,

$$\hat{H} = \hat{H}_{\text{at}} + \hat{H}_{\text{cav}} + \hat{H}_{\text{env}} + \hat{H}_{\text{at-cav}} + \hat{H}_{\text{cav-env}}. \quad (2)$$

The environment is as usual taken as a set of modes of the electromagnetic field

$$\hat{H}_{\text{env}} = \sum_k \nu_k \hat{b}_k^\dagger \hat{b}_k \quad (3)$$

with  $\nu_k$  the mode frequencies and  $\hat{b}_k^\dagger$  ( $\hat{b}_k$ ) the corresponding bosonic creation (annihilation) operators. In the rotating wave approximation (RWA), the cavity-environment coupling is taken as

$$\hat{H}_{\text{cav-env}} = \sum_k \lambda_k (\hat{b}_k^\dagger \hat{a} + \hat{a}^\dagger \hat{b}_k), \quad (4)$$

where  $\hat{a}^\dagger$  ( $\hat{a}$ ) is the creation (annihilation) operator for a cavity photon, and  $\lambda_k$  are the coupling strengths. Following the standard procedure, i.e., assuming the Born-Markov approximation and a moderate atom-field coupling, the Lindblad equation for the atom-cavity system is [19]

$$\begin{aligned} \frac{\partial}{\partial t} \hat{\rho} &= i[\hat{\rho}, \hat{H}_{\text{at}} + \hat{H}_{\text{cav}} + \hat{H}_{\text{at-cav}}] \\ &+ \gamma (2\hat{a} \hat{\rho} \hat{a}^\dagger - \hat{a}^\dagger \hat{a} \hat{\rho} - \hat{\rho} \hat{a}^\dagger \hat{a}) \end{aligned} \quad (5)$$

Here we have assumed that the environment is at zero temperature  $T = 0$ , and  $\gamma$  is the effective photon decay rate.

The idea next is to integrate out the cavity field under suitable conditions to arrive at an effective model for the set of two-level atoms. In order to achieve this we envision the coupling setup schematically presented in Fig. 1. All atoms are identical and couple identically to all light fields, i.e., we disregard spatial variations of the fields. Two stable Zeeman levels  $|1\rangle$  and  $|2\rangle$  are Raman coupled with two classical lasers with amplitudes  $\Omega_1$  and  $\Omega_2$  via a largely detuned excited Zeeman level. In addition, another Raman coupling between the same stable atomic electronic levels is realized with one classical laser with amplitude  $\Omega_3$  and the quantized cavity model with vacuum Rabi frequency  $g$ . This transition is also assumed off-resonant with the intermediate excited atomic state. After adiabatically eliminating of the largely detuned excited states [23] and imposing the RWA, the bare atomic

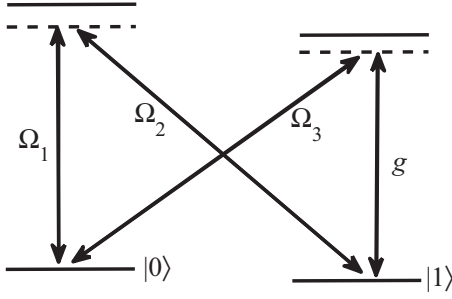


FIG. 1. Atomic-level scheme and coupling configuration demonstrating the two Raman processes; the first is driven resonantly with two classical lasers, marked by  $\Omega_1$  and  $\Omega_2$ , inducing an effective direct coupling between the two stable lower atomic levels  $|1\rangle$  and  $|2\rangle$ , and the second, also resonant, combines a classical laser  $\Omega_3$  with a cavity mode  $g$ . After eliminating the excited, far detuned, atomic hyperfine Zeeman levels we achieve in the RWA two types of couplings between levels  $|1\rangle$  and  $|2\rangle$ , one directly proportional to  $\Omega_1\Omega_2$  and one proportional to  $g\Omega_3$  that is mediated by a cavity photon emission and absorption.

Hamiltonian reads

$$\hat{H}_{\text{at}} = \sum_{i=1}^K \omega \frac{1}{2} (\hat{\sigma}_i^+ + \hat{\sigma}_i^-) = \sum_{i=1}^K \omega \hat{\sigma}_i^x \equiv \omega \hat{S}_x, \quad (6)$$

with  $\hat{\sigma}_i^x$  ( $= |1\rangle\langle 2| + |2\rangle\langle 1|$ ) the  $x$ -Pauli matrix for atom  $i$ ,  $\hat{S}_\alpha = \sum_{i=1}^K \hat{\sigma}_\alpha^{(i)}$  with  $\hat{\sigma}_\alpha^{(i)}$ ,  $\alpha = x, y, z$ , the collective spin operators, and the Rabi frequency  $\omega \sim \Omega_1\Omega_2$ . The atom-cavity interaction is of the Jaynes-Cummings type,

$$\hat{H}_{\text{at-cav}} = G \sum_{i=1}^N (\hat{a}^\dagger \hat{\sigma}_i^- + \hat{a} \hat{\sigma}_i^\dagger), \quad (7)$$

and  $G \sim \Omega_3 g$  and  $\hat{\sigma}_i^\pm$  raising and lowering operators for atom  $i$ . Finally, the bare cavity Hamiltonian is

$$\hat{H}_{\text{cav}} = \nu \hat{a}^\dagger \hat{a}, \quad (8)$$

where  $\nu$  is the photon frequency. In the bad cavity limit,  $\gamma \rightarrow \infty$ , the characteristic timescale for the photons is much shorter than that of the atoms, and we may adiabatically eliminate it to derive an effective model for the atoms alone [23]. The steady-state solution for the boson annihilation operator, considering a zero temperature bath, is [19]

$$\hat{a}_{\text{ss}} = -\frac{iG}{\gamma + i\nu} \hat{S}_-, \quad (9)$$

with  $\hat{S}_- = \sum_{i=1}^N \hat{\sigma}_i^-$ . In the bad cavity limit we may substitute the photon operators of Eq. (5) with their steady states and thereby recover an equation containing only atomic operators. One finds that there is one term  $\sim (\hat{S}_x^2 + \hat{S}_y^2)$  that scales with the loss rate as  $1/\gamma$ , which describes cavity-induced spin flips: one atom emits a photon that is reabsorbed by a second atom. However, this term vanishes as  $\gamma \rightarrow \infty$ , in agreement with that there is no time for the second atom to reabsorb the photon before it is lost to the environment. When neglecting such a photon-induced coupling we arrive at our final model

for the atoms

$$\frac{\partial \hat{\rho}}{\partial t} = i\omega[\hat{\rho}, \hat{S}_x] + \frac{\kappa}{S} (2\hat{S}_- \hat{\rho} \hat{S}_+ - \hat{S}_+ \hat{S}_- \hat{\rho} - \hat{\rho} \hat{S}_+ \hat{S}_+). \quad (10)$$

Here we also introduced the total spin  $S = K/2$ . Note that the strength of the Lindblad coupling  $\kappa \sim G$  can be controlled (as can the Rabi frequency  $\omega$ ) by the amplitudes of the driving lasers, and in particular it does not scale with the photon loss rate in the bad cavity limit. We also note that a very similar scheme as the one proposed above has been realized experimentally [24]. In that experiment a high- $Q$  cavity was considered, and consequently to realize the dissipative transition discussed here one would need a larger photon loss rate  $\gamma$ . Too large of a  $\gamma$  may, however, soften the well-defined cavity mode frequencies, and the atoms could couple to multiple cavity modes. This is most likely not a severe drawback since we need not care about the details of the cavity after eliminating it. Of course, this would probably renormalize the coupling parameter  $\kappa$ . Furthermore, including counter-rotating terms in the atom-cavity coupling will result in additional atomic Lindblad terms, but these should be negligible in the optical regime where we expect the RWA to be justified.

We end this subsection with a general remark about fully connected models like the one of Eq. (10). We note that the ideas of scale invariance and local order parameters rely on local Hamiltonians, e.g., tight-binding models. At the critical point the characteristic length diverges as  $\xi^{-1} \sim |g - g_c|^\lambda$  and the energy gap closes as  $\Delta \sim |g - g_c|^{z\lambda}$  for the dynamical critical exponent  $z$  [8]. For “fully connected models,” i.e., all particles are connected, locality is in a strict sense lost. Nevertheless, it is still possible to show scale invariance and also to introduce a counterpart of  $\xi$  that has been termed the “coherence number” [25]. In addition, we can still talk about local observables provided that it can be expressed as a sum  $\hat{O} = \sum_i \hat{o}_i$  where  $\hat{o}_i$  is restricted to act on particle  $i$ . For a continuous phase transition we thereby require that all local  $\hat{O}$ 's are continuous.

### C. Steady-state solution

The model of Eq. (10) was frequently discussed in the late 1970s in terms of cooperative emission of radiation and how this relates to optical bistability [26,27]. The model is analytically solvable in the sense that the (unique) steady state is obtainable [28]. The Hamiltonian alone,  $\hat{H} = \omega \hat{S}_x$ , is trivial, and likewise is the Lindblad part of Eq. (10) on its own. Energetically the Hamiltonian supports the state  $|S, -S\rangle_x$  (the spins pointing down along the  $x$  direction), while the dissipation pushes the state towards  $|S, -S\rangle_z$  (the spins pointing down along the  $z$  direction). Any phase transition between these limiting states is a result of the interplay between the unitary and dissipative parts of the model; note especially that  $[\hat{S}_x, \hat{S}_-] \neq 0$ .

The total spin is preserved for Eq. (10), and its unique steady state can be expressed in terms of the spin operators as [28]

$$\hat{\rho}_{\text{ss}} = \hat{\eta} \hat{\eta}^\dagger, \quad (11)$$

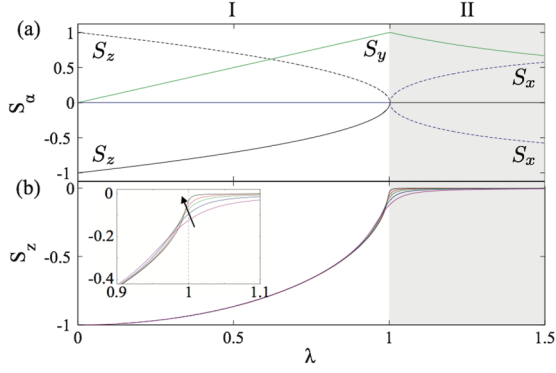


FIG. 2. Mean-field (a) and full quantum steady-state solutions (b) as a function of  $\lambda$ . For the mean-field expectations,  $S_x$ ,  $S_y$ , and  $S_z$  are marked in the plot with blue, green, and black, respectively; the solid lines represent stable solutions and the dashed ones unstable. The two phases, magnetized and paramagnetic, are marked by I and II (gray shaded), respectively. In (b) the different curves give the magnetization  $S_z$  for different spins:  $S = 50$ ,  $S = 100$ ,  $S = 200$ ,  $S = 400$ , and  $S = 1600$ . The inset shows a closeup of  $S_z$  in the vicinity of the critical coupling, and the arrow indicates the growing spin sizes  $S$ .

where  $\hat{\eta} = \frac{1}{\sqrt{D}} \sum_{n=0}^{2S} \left(\frac{\hat{S}_z}{g^n}\right)^n$ ,  $g = i\omega S/\kappa$ , and the normalization

$$D = \sum_{m=0}^{2S} \frac{(2S+m+1)!(m!)^2}{(2S-m)!(2m+1)!} |g|^{-2m}. \quad (12)$$

Various expectations for these exact quantum solutions are shown in Fig. 2 for different system sizes. In particular, they are compared to the mean-field solutions derived in the next section. We may note that the model possesses the dual spectral ‘‘symmetry’’  $\omega \rightarrow -\omega$  and  $\hat{S}_- \leftrightarrow \hat{S}_+$  with corresponding steady state as (11) with the raising and lowering operators interchanged.

### III. RESULTS AND DISCUSSIONS

#### A. Mean-field analysis

##### 1. Mean-field solutions

The thermodynamic limit  $S \rightarrow \infty$  is usually associated with the classical limit of the spin, and we thereby expect mean-field methods to correctly predict, for example, critical exponents. Hence, quantum fluctuations alone cannot cause the destabilization of the different phases, which is indeed not uncommon for fully connected models [29].

In the simplest mean-field picture, quantum correlations are fully discarded, and we treat operators as commuting quantities. By normal ordering the equations, this is equivalent to assigning a coherent state ansatz of the state. The resulting equations of motion follow from  $\partial_t O \equiv \partial_t \langle \hat{O} \rangle = \text{Tr}[\hat{O} \partial_t \hat{\rho}]$  for any operator  $\hat{O}$ , e.g., for the spin variables

$$\begin{aligned} \frac{\partial S_x}{\partial t} &= 2\frac{\kappa}{S} S_x S_z, \\ \frac{\partial S_y}{\partial t} &= -\omega S_z + 2\frac{\kappa}{S} S_y S_z, \\ \frac{\partial S_z}{\partial t} &= \omega S_y - 2\frac{\kappa}{S} (S_x^2 + S_y^2). \end{aligned} \quad (13)$$

The steady-state solutions (fixed points) for  $\lambda \equiv \omega/2\kappa \leq 1$ , taking into account that the total spin is preserved, are

$$(S_x, S_y, S_z) = S(0, \lambda, \pm\sqrt{1-\lambda^2}). \quad (14)$$

In this regime the system builds up a finite magnetization, and we thereby call the phase magnetized. The solution  $S_z = -\sqrt{1-\lambda^2}$  turns out stable and with the other unstable (see the next subsection). In the parameter regime  $\lambda \geq 1$  where the magnetization vanishes, i.e., a paramagnetic phase, the steady states are

$$(S_x, S_y, S_z) = S(\pm\sqrt{1-1/\lambda^2}, 1/\lambda, 0). \quad (15)$$

Here, however, the solutions are not stable (again, see the next subsection). In fact, neither of the above bifurcations agrees with the more familiar ones, e.g., pitchfork or Hopf bifurcations [30]. For example, the branches  $S_x = \pm\sqrt{1-1/\lambda^2}$  have purely imaginary eigenvalues, but this is still not representing a Hopf bifurcation in the sense that the solutions do not approach limit cycles. At this level of mean-field study, the absence of a stable steady state for  $\lambda > 1$  is clearly in contrast to the full quantum solution (11). Similar observations have been found for optical bistability, where on a mean-field level the solutions form a saddle-node bifurcation, while the full quantum solution does not show the typical hysteresis behavior [17]. The steady-state solutions (14) and (15) and their stabilities are depicted in Fig. 2(a), while in Fig. 2(b) we depict the corresponding finite system size quantum solutions.

#### 2. Mean-field stability analysis

The stability of the steady-state solutions, Eqs. (14) and (15), is given by linearizing around these solutions and exploring the eigenvalues of the corresponding Jacobian [30]. Since the total spin is preserved, it is convenient to turn to the canonical variables  $(z, \phi) = (\cos \theta, \phi)$ , for which the equations of motion become

$$\begin{aligned} \frac{\partial z}{\partial t} &= -2\kappa(1-z^2) + \omega\sqrt{1-z^2} \sin \phi, \\ \frac{\partial \phi}{\partial t} &= -\omega \frac{z}{\sqrt{1-z^2}} \cos \phi. \end{aligned} \quad (16)$$

$\theta$  and  $\phi$  are the polar and azimuthal angles, and note that  $z$  is identical to the magnetization  $S_z$ . In the canonical variables the fixed points (14) and (15) are

$$(\theta, \phi) = (\pm\sqrt{1-z^2}, \pi/2), \quad (17)$$

for  $0 \leq \lambda \leq 1$ , and

$$(\theta, \phi) = (\pi/2, \pm\sqrt{1-z^2}), \quad (18)$$

for  $\lambda \geq 1$ .

The Jacobian corresponding to solutions (17) is given by

$$J = \begin{bmatrix} \pm 2\kappa\sqrt{1-\lambda} & 0 \\ 0 & \pm 2\kappa\sqrt{1-\lambda} \end{bmatrix}, \quad (19)$$

and it is clear that only the second solution gives negative eigenvalues and is thereby stable. Thus, while the solutions are symmetric under the reflection  $S_z \leftrightarrow -S_z$ , the results from the stability analysis show that the two solutions are qualitatively different, which prohibits any such parity symmetry.

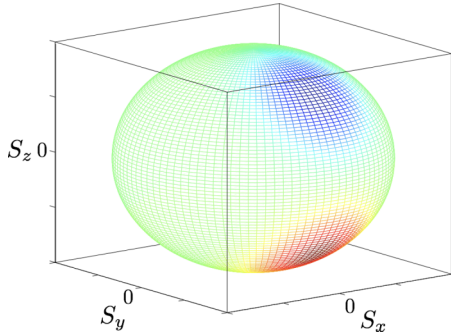


FIG. 3. A schematic figure demonstrating the idea of one “repulsive” (unstable) one “attractive” (stable) fixed point on the phase space of the spin. This plot corresponds to a coupling  $\lambda = 0.35$  where the fixed points are somewhere between the north (south) and east poles. The system approaches the stable fixed point in a finite time regardless of its initial state. On a flat phase space there would be a small set of initial states that would not reach the stable fixed point in a finite time.

The remaining two solutions, Eq. (18), give the Jacobian

$$J = \begin{bmatrix} 0 & \pm\omega\sqrt{1-\lambda^{-1}} \\ \mp\omega\sqrt{1-\lambda^{-1}} & 0 \end{bmatrix} \quad (20)$$

with purely imaginary eigenvalues. This is reminiscent of a Hopf bifurcation, but contrary to a Hopf here the trajectories do not approach limit cycles [30]. The appearance of periodic solutions for  $\lambda > 1$  was already predicted in Ref. [26] using a Fokker-Planck method for the Glauber distribution. But the actual steady states were not identified in that reference.

The equations for  $z$  and  $\phi$  cannot be put on a “potential form,” i.e.,  $\frac{\partial z}{\partial t} = \frac{\partial V(z, \phi)}{\partial \phi}$  and  $\frac{\partial \phi}{\partial t} = -\frac{\partial V(z, \phi)}{\partial z}$ . This, of course, derives from the dissipative nature of the problem. We may, however, schematically think of the fixed points as attractors or repellers on the phase space. Since the phase space is a sphere, in the magnetized phase we should envision one repulsive and one attractive point in the sphere along the  $yz$  meridian, as illustrated in Fig. 3. Numerically we have verified that for random initial states, in a rather short time, the state approaches the stable fixed point. This fast relaxation of general states is possible only due to the geometry of the phase space. On the plane, with one attractive and one repulsive fixed point, one would most likely find some states that relax infinitely slowly. The phase space geometry together with that the model is dissipative most likely explain that the bifurcation is not one of the standard ones found in textbooks.

### B. Critical exponents

The theory of phase transitions predicts universal critical behavior that can be ascribed a few critical exponents [1]. For a symmetry-breaking continuous phase transition we expect that sufficiently close to the critical point any local observable

$$\langle \hat{O} \rangle \propto |\lambda - \lambda_c|^{\beta_{\pm}}, \quad (21)$$

where  $\beta_{\pm}$  is the exponent depending on if the critical point is approached from above or below, i.e., the behavior need not be symmetric. It is unclear whether our phase transition should obey the same universality, even if it is likely

that the found nonanalyticity also has an algebraic structure like (21). As pointed out above, by “local” in our model we mean that  $\hat{O} = \sum_i \hat{o}_i$  with  $\hat{o}_i$  a single-particle operator acting on atom  $i$ . In more general terms, for operators  $\hat{C} = \sum_i \sum_j \dots \sum_k \hat{a}_i \hat{b}_j \dots \hat{c}_k$  expanded in single-particle operators we define “locality” by the number of single-particle operators in the product  $\hat{a}_i \hat{b}_j \dots \hat{c}_k$ .

It is clear that the critical point of our model occurs for  $\lambda_c = 1$ , and that the mean-field critical exponent for the magnetization  $S_z \delta = 1/2$ . Furthermore, the negative eigenvalues of the Jacobian (19) define the timescale for relaxing to the steady state (in the validity regime for the linear expansion). This tells us that the gap  $\Delta$  of the Liouvillian  $\hat{\mathcal{L}}$  closes as  $\Delta \propto \kappa\sqrt{1-\lambda}$ , i.e., the characteristic timescale  $T \propto (1-\lambda)^{-1/2}$ . The inset of Fig. 2(b) shows a closeup of the magnetization around the critical point for different system sizes. It suggests that the mean-field exponent  $\delta = 1/2$  becomes exact in the thermodynamic limit as expected (we have checked this more systematically via a scaling analysis and indeed found the critical exponent  $\delta = 1/2$ ).

The spin variances

$$\Delta S_{\alpha} = \langle \hat{S}_{\alpha}^2 \rangle - \langle \hat{S}_{\alpha} \rangle^2, \quad \alpha = x, y, z \quad (22)$$

are examples of the most weakly nonlocal operators, containing only products of single-particle operators. The three variances for different  $S$  are displayed in Fig. 4(a), and the corresponding exponents in Fig. 4(b). By extrapolating the results to  $S = \infty$  the three exponents seem to attain different values and in particular not simple fractional values (see the figure caption). Normally for fully connected models the mean-field results are correct, and one could expect simple fractions for the exponents. In the present model we have seen, however, that in the paramagnetic phase the mean-field results do not agree with the full quantum ones; we find different steady states. Note that to derive the mean-field exponents for the variances one would need to go beyond the simple factorization of operators to include products of operators.

We may also consider maximally delocalized observables, which do not need to be continuous at the critical point. In Fig. 5(a) the purity [31]

$$P = \text{Tr}[\hat{\rho}_{\text{ss}}^2] \quad (23)$$

is plotted. The purity is a measure of how mixed the state is, with  $P = 1$  representing a pure state and  $P = 1/(2S + 1)$  representing the fully mixed state (i.e., the density operator proportional to the identity matrix). We may alternatively interpret the purity as the expectation of the state itself,  $P = \langle \hat{\rho}_{\text{ss}} \rangle$ . As we see in the figure, when  $S \rightarrow \infty$   $P$  becomes discontinuous and jumps from  $P = 1$  in the magnetized phase to  $P = 0$  in the paramagnetic phase. This is thereby an example of an extrinsic quantity that is not continuous across the critical point. Similar examples can be found in equilibrium quantum phase transitions like the fidelity susceptibility [32]. If we would instead consider the purity  $P_q$  for a single qubit [see Eq. (27) below], this is a local operator, and we should not encounter a discontinuity. This is confirmed in Fig. 5(b), and we in particular see the characteristic cusplike behavior for a continuous phase transition as  $S \rightarrow \infty$ . This purity is defined similarly;  $P_q = \text{Tr}[\hat{\rho}_q^2]$  with  $\hat{\rho}_q$  the reduced density

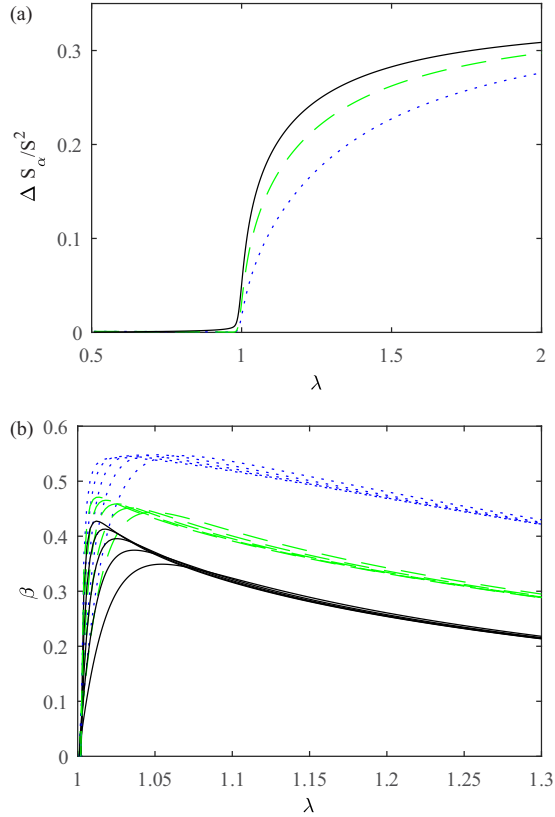


FIG. 4. The spin variances  $\Delta S_\alpha$  ( $\alpha = x, y, z$ , dotted blue, dashed green, and solid black, respectively) (a) and their respective exponents (b) as a function of  $\lambda$ . The different curves in (b) are the results for  $S = 50, 100, 200, 400, 1600$ , and in (a)  $S = 400$ . By extrapolating the results of (b) to  $S = \infty$  one finds  $\beta_x \approx 0.54$ ,  $\beta_y \approx 0.48$ , and  $\beta_z \approx 0.46$  at the critical point.

operator for a single qubit. A similar behavior is also found for the purity for a two-qubit state (not shown here), but with a slightly “sharper” emerging discontinuity.

### C. Quantum properties of $\hat{\rho}_{ss}$

It has been shown that the scaling of entanglement properties for continuous phase transitions is universal [33]. In particular, the entanglement is maximized at the critical point, for both short and infinite range models. For fully connected models, where mean-field predictions give the correct exponents, nontrivial quantum correlations may exist away from the critical point also in the thermodynamic limit [34]. In the present model, where the continuous phase transition emerges from a first-order phase transition, it is not known how entanglement will depend upon approaching the critical point. Moreover, the criticality itself derives from large fluctuations from the system’s intrinsic open character, and one could therefore expect them to completely demolish any quantum correlations in the thermodynamic limit.

By fully characterizing the entanglement of a multipartite state we would need to partition it in all possible ways and calculate the corresponding entanglement between its constituents. Here we focus on qubit-qubit entanglement mea-

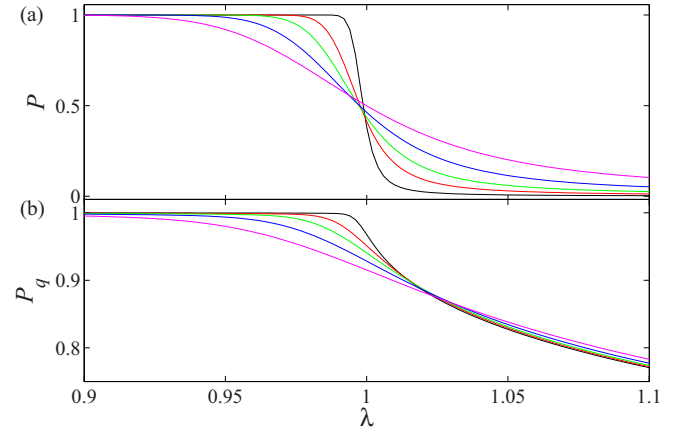


FIG. 5. Purities for the full state  $\hat{\rho}_{ss}$  (a) and the single-qubit reduced state  $\hat{\rho}_q$  (b) for the same spin sizes  $S$  as in Fig. 4 (the arrow again points in the direction of growing  $S$ ). In the thermodynamic limit  $S \rightarrow \infty$ , the purity of the state  $\hat{\rho}_{ss}$  shows a steplike behavior going from a pure to a maximally mixed state. In the same limit the reduced single-particle state stays continuous with, however, a cusplike behavior.

sured by the negativity [35]

$$\mathcal{N} = \sum_i \frac{|\mu_i| - \mu_i}{2}, \quad (24)$$

where  $\mu_i$  is the  $i$ th eigenvalue of the partially transposed reduced density operator  $\hat{\rho}_{2q}^{T_A}$  for the two qubits. Negativity is both a necessary and sufficient condition to quantify entanglement for pairwise mixed qubit states. As a symmetric state,  $\mathcal{N}$  is numerically easy to calculate [36]. In particular the reduced state becomes

$$\hat{\rho}_{2q} = \begin{bmatrix} v_+ & x_+^* & x_+^* & u^* \\ x_+ & w & w & x_-^* \\ x_+ & w & w & x_-^* \\ u & x_- & x_- & v_- \end{bmatrix}, \quad (25)$$

with the elements expressed in the collective spin expectations

$$\begin{aligned} v_\pm &= \frac{S^2 - S + \langle \hat{S}_z^2 \rangle \pm 2\langle \hat{S}_z \rangle (S - 1/2)}{4(S - 1/2)}, \\ x_\pm &= \frac{2(S - 1/2)\langle \hat{S}_+ \rangle \pm \langle [\hat{S}_+, \hat{S}_z]_+ \rangle}{8(S - 1/2)}, \\ w &= \frac{S^2 - \langle \hat{S}_z^2 \rangle}{4S(S - 1/2)}, \\ u &= \frac{\langle \hat{S}_+^2 \rangle}{4S(S - 1/2)}. \end{aligned} \quad (26)$$

From Eq. (25) one also directly obtains the single-qubit reduced density operator

$$\hat{\rho}_q = \begin{bmatrix} w + v_+ & x_+^* + x_-^* \\ x_+ + x_- & w + v_- \end{bmatrix}. \quad (27)$$

The result for the scaled negativity  $N = \mathcal{N}/\max(\mathcal{N})$  is shown in Fig. 6(a) for different system sizes. Away from the critical point ( $\lambda < 1$ ), the negativity scales as  $\mathcal{N} \sim S^{-1}$  with the system size, while for the maximum  $\max(\mathcal{N}) \sim S^{-0.9}$  such that

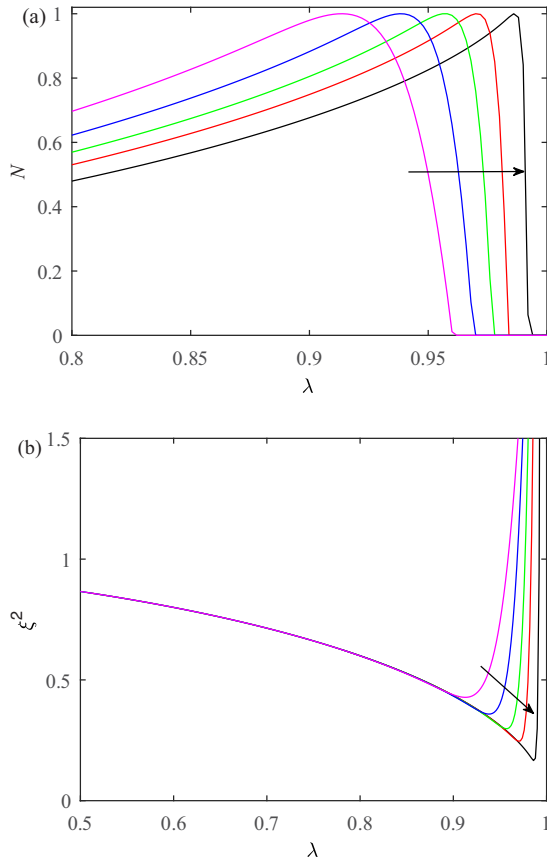


FIG. 6. Normalized negativity  $N = \mathcal{N}/\max(\mathcal{N})$  (a) as a measure of qubit-qubit entanglement and full state spin  $x$ -squeezing (b). The spin sizes are the same as Fig. 5, with the arrow indicating growing spin sizes. As  $S \rightarrow \infty$  the entanglement peaks at the critical point  $\lambda = 1$ . For smaller values of  $\lambda$  the negativity goes asymptotically to zero. The squeezing is also maximum at the critical point  $\lambda = 1$  as  $S \rightarrow \infty$ , and all squeezing is lost beyond the critical point  $\lambda > 1$  in the paramagnetic phase.

it actually vanishes identically in the thermodynamic limit. The inverse scaling  $\sim S^{-1}$  demonstrates the phenomenon of “shared entanglement,” which states that a large entanglement cannot be obtained among all constituents simultaneously [37].

From Fig. 5(b) it is seen that in the thermodynamic limit the reduced density operators are pure in the magnetized phase and continuously become more and more mixed in the paramagnetic phase. At the same time, we saw in Fig. 6(a) that qubit-qubit entanglement vanishes in the paramagnetic phase for any  $S$ . The fact that  $P_q = 1$  in the thermodynamic limit in the magnetized phase indicates that there are no quantum correlations surviving as  $S \rightarrow \infty$ . To explore this further we consider the spin squeezing [38]

$$\xi^2 = \frac{2S\Delta S_{n_1}^2}{\langle \hat{S}_{n_2} \rangle^2 + \langle \hat{S}_{n_3} \rangle^2}. \quad (28)$$

Here  $n_1, n_2$ , and  $n_3$  could in principle be any three orthogonal vectors, but we restrict ourselves to  $x, y$ , and  $z$ . Whenever  $\xi^2 < 1$  the state is squeezed, and since spin squeezing acts as an entanglement witness, the state must be entangled [38,39].

That means that if  $\xi^2 < 1$ , the state cannot be composed as a product state, and hence it embodies some sort of quantum correlations. For  $n_1 = y, z$  one finds that  $\xi^2 > 1$  for any  $S$  and  $\lambda$ . However, as demonstrated in Fig. 6(b), for  $n_1 = x$   $\xi^2 < 1$  whenever  $\lambda < 1$  and for all  $S$ , and the state is indeed entangled. In the thermodynamic limit maximum squeezing is obtained at the critical point, and for smaller couplings  $\lambda$  the dependence on  $S$  is very weak, meaning that the number of multipartite correlations in the state remains when  $S$  is increased. At first this seems to contradict the results of Fig. 5(b). However, it must be remembered that  $\xi^2$  says something about the total number of quantum correlations, while the purity is for single qubits, and thus even though the state factorizes in the limit  $S \rightarrow \infty$ , as long as  $S$  is finite the state is not an exact product state, and it comprises the finite full state entanglement. The fact that both the negativity, and the squeezing, have a peak at the critical point [22,40] is in agreement with the general behavior of continuous quantum phase transitions [33].

#### D. Absence of symmetry breaking

It is found that  $S_z$  obeys the typical behavior for a continuous phase transition; it has a discontinuous first derivative, and close to the critical point it is determined by a critical exponent. In fact, any local observable will be continuous. As a continuous phase transition, and if the system would obey the Landau paradigm, we expect an accompanying symmetry breaking. In contrast to Hamiltonian systems, for an irreversible master equation such as the Lindblad one, a symmetry does not automatically define a preserved quantity. More precisely, a symmetry for a Lindblad master equation is defined as invariance of the Liouvillian  $\hat{\mathcal{L}}$  under some unitary  $\hat{U}$ , i.e.,  $\hat{\mathcal{L}}$  is not altered by  $\hat{H} \rightarrow \hat{U}\hat{H}\hat{U}$  and  $\hat{L}_i \rightarrow \hat{U}\hat{L}_i\hat{U}$  [41]. The steady-state solutions (14) and (15) are symmetric under a  $\pi$  rotation around  $S_y$ ,  $S_x \leftrightarrow -S_x$  and  $S_z \leftrightarrow -S_z$ . This is exactly the aforementioned dual “symmetry,” but it is evidently not a true symmetry since the two solutions have different stability properties. In fact, our model lacks symmetries.

Symmetries are naturally also reflected in the phase space distributions. For a  $\mathbb{Z}_2$  symmetry, for example, one finds for the ground state two blobs with interferences in between. Thus, by mapping out the phase space distributions as a function of  $\lambda$  one can identify the phase transition and visualize possible accompanying symmetry breaking. In NESS phase transitions where a symmetry breaking occurs one typically encounters the same qualitative behavior; see, for example, Ref. [42]. On the other hand, without any symmetries one should only find a single blob in the phase space distribution regardless of the phase. However, once crossing the critical point from the magnetized phase, fluctuations should greatly set in and start to smear out the distribution. As a demonstration, we consider the  $SU(2)$   $Q$  function defined as [43]

$$Q(z) = \langle z | \hat{\rho} | z \rangle, \quad (29)$$

with the spin coherent state [44]

$$|z\rangle = \frac{1}{(1+|z|^2)^j} \sum_{m=-S}^S \sqrt{\binom{K}{S+m}} z^{S+m} |S, m\rangle, \quad (30)$$

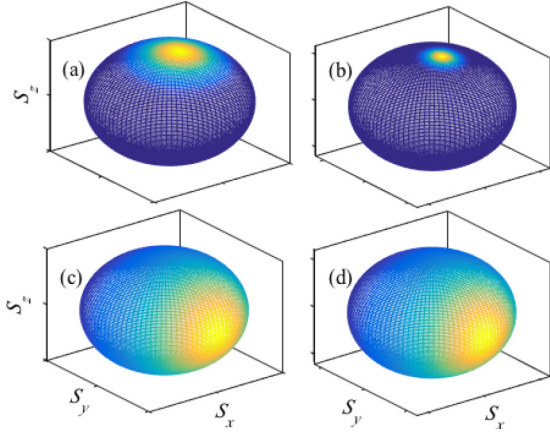


FIG. 7. The Husimi  $Q$  function for  $\lambda = 0.05$  (a, b) and  $\lambda = 1.05$  (c, d). For the left panel  $S = 10$ , and  $S = 100$  for the right panel. In the first two plots, in the magnetized phase, the state is approximately pure and the fluctuations are quantum. This is particularly demonstrated in the decreasing number of fluctuations for increasing  $S$ : in the thermodynamic (classical) limit  $S \rightarrow \infty$  the distribution would collapse to a single point on the phase space. The last two plots depict the distributions in the paramagnetic phase, and evidently the number of fluctuations is considerably larger. These stem from the openness of the model, and in particular as  $\lambda \rightarrow \infty$  or  $S \rightarrow \infty$  the state is maximally mixed and the corresponding  $Q$  function will be smeared out entirely over the sphere. The  $z$  axis has been flipped in order to better visualize the distribution.

where  $z = e^{i\phi} \tan \frac{\theta}{2}$  and  $|S, m\rangle$  is the spin angular momentum state with  $z$ -quantum number  $m$ . The results for the  $Q$  function for two different spins are shown in Fig. 7 (see also Ref. [40]). We indeed see no indications of a symmetry breaking, and it confirms the picture of fluctuations blowing up in the incoherent paramagnetic phase. In particular, to a good agreement the size of  $S$  determines only the number of fluctuations in the magnetized phase where we know that in the classical limit  $S \rightarrow \infty$  the distribution collapses into a single point.

Let us now present a picture of how the continuous transition emerges despite no symmetry breaking. The full system, discussed in Sec. II B, resembles the open Dicke model [9], with an additional pump term that breaks the  $\mathbb{Z}_2$  parity symmetry characteristic for the Dicke model [29,45,46]. This leaves a system lacking any symmetries, and what one finds is instead a first-order phase transition that can be identified with optical bistability [14,15]. Optical bistability manifests as two stable coexisting mean-field steady-state solutions for a given pump strength. However, at a quantum level fluctuations cause an inherent self-averaging of the two solutions such that a single unique steady state is found which shows a sudden jump for some critical pump, i.e., it realizes a NESS first-order phase transition [15,17]. The mean-field solutions survive dynamically as long-lived metastable states in which the system can jump between due to the fluctuations. In our situation, even at a mean-field level the bistability is quenched into a continuous transition, and it is thereby conceptually different from earlier results on optical bistability, not only from the fact that it is continu-

ous rather than discontinuous. We note that for equilibrium classical phase transitions, the passage between first-order and continuous phase transitions can result from fluctuations or disorder [4]. For the Potts model or the classical  $XY$  model, it is also known that the order of the phase transition can depend on system variables, changing from first to second order [47], and moreover that the emergent continuous transitions can be characterized by critical exponents. In the bad cavity limit, environment-induced fluctuations vastly increase, and it seems that this is what is causing the transition to turn from a first-order to a continuous one.

Returning to the Dicke model, at the mean-field level it is known that the Dicke model is critical also for finite photon losses  $\gamma$ . However, in the bad cavity limit  $\gamma \rightarrow \infty$ , the critical coupling becomes infinite [29,45]. This is understood from the fact that the term describing photon-mediated atom-atom coupling vanishes in this limit, and it is this term driving the Dicke phase transition. There is, however, one important point to be clarified: in the Dicke model there is a term  $\Delta \hat{S}_z / 2$  which vanishes in our model as we assume a resonant Raman coupling between the two levels  $|1\rangle$  and  $|2\rangle$  (see Sec. II B). The critical coupling of the Dicke model is [29,45]

$$G_c = \frac{1}{2} \sqrt{\frac{\Delta}{\nu} (\nu^2 + \gamma^2)}, \quad (31)$$

such that for  $G < G_c$  the photon field is in an approximate vacuum and the spin points to the south pole, and for  $G > G_c$ , the superradiant phase, both the field and the atoms get macroscopically excited. Note that if we artificially impose the scaling  $\Delta \rightarrow \Delta / \gamma^2$ , the critical coupling stays finite in the bad cavity limit.

When we let the Rabi frequency  $\omega = 0$  in our model, i.e., turning off one of the Raman couplings, the Hamiltonian possesses a global continuous  $U(1)$  symmetry corresponding to particle conservation. Even when giving up the RWA, there is a  $\mathbb{Z}_2$  parity symmetry that emerges for  $\omega = 0$ . This symmetry is spontaneously broken in the Dicke phase transition, regardless of whether it is an open or closed model. We may think of the pump term  $\omega \hat{S}_x$  as a transverse field that breaks this symmetry such that the total Hamiltonian is left with no symmetries. As a result, we are left with a Hamiltonian lacking any symmetries, and we thereby cannot expect a continuous symmetry breaking to occur. So how is it that we can see a continuous phase transition at all in our effective model for the atoms?

It has long been known that the closed Dicke model with a pump term still supports a phase transition [48], but it is no longer second order but first order. Thus, upon changing the pump amplitude the system's steady state may make a sudden jump manifested, for example, in a discontinuity in the cavity field amplitude. Let us analyze the open pumped Dicke model with the scaling discussed above:

$$\hat{H}_{\text{Dicke}} = \nu \hat{a}^\dagger \hat{a} + \frac{\Delta}{2\gamma^2} \hat{S}_z + \omega \hat{S}_x + \frac{G}{\sqrt{K}} (\hat{a}^\dagger + \hat{a}) \hat{S}_x. \quad (32)$$

In the quadrature representation,  $\hat{x} = (\hat{a}^\dagger + \hat{a}) / \sqrt{2}$  and  $\hat{p} = i(\hat{a}^\dagger - \hat{a}) / \sqrt{2}$ , the mean-field equations of motion



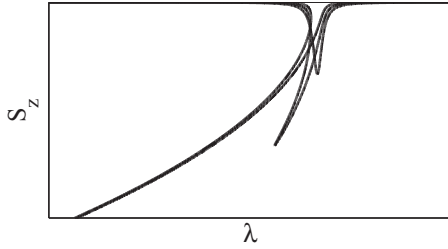


FIG. 8. Simplified illustration how bistability (first-order phase transition) turns into a continuous phase transition. For weak photon losses  $\gamma$  there is a one-to-one mapping between  $\lambda$  and the magnetization  $S_z$ . Beyond some coupling the system builds up multiple solutions, and by varying  $\lambda$  the system would show hysteresis. The larger  $\gamma$  gets, the more close the two solutions, and finally in the limit  $\gamma \rightarrow \infty$  the curves merge and a nonanalyticity appears at the critical point. We point out that the figure is only for an informative description and should not be taken as a faithful representation of our system.

read [29,45]

$$\begin{aligned}
 \frac{\partial x}{\partial t} &= \nu p - \gamma x, \\
 \frac{\partial p}{\partial t} &= -\nu x - \frac{2G}{\sqrt{K}} S_x - \gamma p, \\
 \frac{\partial S_x}{\partial t} &= -\frac{\Delta}{2\gamma^2} S_y, \\
 \frac{\partial S_y}{\partial t} &= \frac{\Delta}{2\gamma^2} S_x - \left( \frac{2Gx}{\sqrt{K}} + \omega \right) S_z, \\
 \frac{\partial S_z}{\partial t} &= \left( \frac{2Gx}{\sqrt{K}} + \omega \right) S_y.
 \end{aligned} \tag{33}$$

The analytic expressions for the steady-state solutions are lengthy and not very informative. Nevertheless, for finite  $\gamma$  one typically finds hysteresis behavior (optical bistability) that is often taken as the mean-field precursor of first-order phase transitions. It is interesting, however, that in the bad cavity limit,  $\gamma \rightarrow \infty$ , the two stable solutions merge and the first-order transition transforms into a continuous one just as found in our effective model [Eq. (2)].

The above mean-field analysis suggests that the absence of symmetry breaking in our continuous phase transition derives from the fact that the transition is a remnant of a first-order phase transition. More precisely, in the bad cavity limit the first-order phase transition turns into a continuous one. This is schematically depicted in Fig. 8; as  $\gamma$  increases the curve begins to tilt over, and above a certain  $\gamma_c$  one finds three solutions for the magnetization signaling hysteresis, and as  $\gamma$  gets even larger the distance between the two curves narrows down and the curves stretch out to mimic more a continuous phase transition. However, it should be stressed that both the figure and the above analysis are rather simplified. Indeed, the analysis does not quantitatively reproduce the expectations of our model (Fig. 1). This is particularly clear when substituting the steady state  $x = -2G/\sqrt{K}(\nu + \gamma^2/\nu)$  into the last two equations of (33). The resulting equations of motion for the spin do not have the same structure as those of the actual

model, Eq. (10). In fact, up to order  $O(K^{-1})$  such a substitution generates an infinite range Ising type interaction  $\sim \hat{S}_x^2$ , and the resulting effective spin dynamics is Hamiltonian [49]. Thus, such an approach does not take dissipative evolution into account and one should instead consider the scheme explained in Sec. II B, i.e., substitute the photon steady states into the master equation instead of the mean-field equations of motion.

#### IV. CONCLUSION

In this work we considered a driven-dissipative quantum system that shows evidence of a continuous phase transition in terms of emergent nonanalytic behaviors in the thermodynamic limit in both the system state and local observables. Still the transition cannot be tied to a symmetry breaking as in the Landau theory of continuous phase transitions. This is in contrast to the related dissipative Lipkin-Meshkov-Glick model, which supports a NESS phase transition that breaks a parity symmetry [40,50]. We argued that the transition stems from a first-order phase transition that dissolves into a continuous transition in the bad cavity limit; large environment-induced fluctuations smear out the discontinuous phase transition. Indeed, the crossover between discontinuous and continuous phase transitions is known from classical systems and derives from large fluctuations. Thus, our results indicate that similar behavior can also be envisioned in nonequilibrium quantum phase transitions. In addition, it also predicts a type of optical bistability that would not manifest as sudden jumps in the cavity output field.

In order to characterize the properties of the transition, we introduced a “local” order parameter in the magnetization, but it should not be taken as an order parameter in the strict sense since it cannot be associated to a symmetry in the first place. Recently the physics behind symmetry breaking in dissipation-driven phase transitions has been explored [51]. Why the present model does not belong to their rather general results is because it does not support a symmetry to start with, i.e., one can observe continuous NESS phase transitions even in systems lacking symmetries. Our critical behavior is conceptually different from other classical systems where nonequilibrium phase transitions may take place without breaking of any symmetry as there the transitions are typically dynamical, which means that the system evolution can display nonanalytic behavior upon changing some parameter [52]. As a next step, our results should be tested on more general grounds, e.g., not for a fully connected model but a local one, for example, those of Ref. [12]. Due to similarities with the present model we believe that the same type of behavior will be recovered also in those models.

The physical realization of our model was discussed in Sec. II B, and with the present experiments with cold atomic condensates loaded in optical resonators [53] or Raman coupled cold atomic gases [24,54] it should indeed be possible to reach the critical point with these setups. Moreover, the magnetization  $S_z$  is directly measurable via either time-of-flight detection or fluorescence detection in the two respective experiments. Measuring other local observables follows directly from applying the desirable pulses first [55].

## ACKNOWLEDGMENTS

We thank Gerard Milburn, Thomas Kvorning, and Chitanya Joshi for helpful discussions. We acknowledge financial support from the Knut and Alice Wallenberg Foundation (KAW) and the Swedish Research Council (VR).

- 
- [1] N. Goldenfeld, *Lectures on Phase Transitions and the Renormalization Group* (Perseus Books, Reading, MA, 1992); J. Cardy, *Scaling and Renormalization in Statistical Physics* (Cambridge University Press, Cambridge, 1996).
- [2] M. Plischke and B. Bergersen, *Equilibrium Statistical Physics* (World Scientific, Singapore, 2006).
- [3] S. Murakami, *New J. Phys.* **10**, 029802 (2008); L. Tsui, Y.-T. Huang, H.-C. Jiang, and D.-H. Lee, *Nucl. Phys. B* **919**, 470 (2017).
- [4] S. Alexander, *Solid State Commun.* **14**, 1069 (1974); M. Aizenman and J. Wehr, *Phys. Rev. Lett.* **62**, 2503 (1989).
- [5] M. Müller, S. Diehl, G. Pupillo, and P. Zoller, *Adv. At. Mol. Opt. Phys.* **61**, 1 (2012); J. Marino and S. Diehl, *Phys. Rev. Lett.* **116**, 070407 (2016).
- [6] M. Fitzpatrick, N. M. Sundaresan, A. C. Y. Li, J. Koch, and A. A. Houck, *Phys. Rev. X* **7**, 011016 (2017); J. M. Fink, A. Dombi, A. Vukics, A. Wallraff, and P. Domokos, *ibid.* **7**, 011012 (2017).
- [7] J. T. Barreiro, M. Müller, P. Schindler, D. Nigg, T. Monz, M. Chwalla, M. Hennrich, C. F. Roos, P. Zoller, and R. Blatt, *Nature (London)* **470**, 486 (2011); Y. Lin, J. P. Gaebler, F. Reiter, T. R. Tan, R. Bowler, A. S. Sorensen, D. Leibfried, and D. J. Wineland, *ibid.* **504**, 415 (2013).
- [8] S. Sachdev, *Quantum Phase Transitions* (Cambridge University Press, Cambridge, 2011).
- [9] B. Öztop, M. Bordyuh, Ö. E. Müstecaploğlu, and H. E. Türeci, *New J. Phys.* **14**, 085011 (2012); D. Nagy and P. Domokos, *Phys. Rev. Lett.* **115**, 043601 (2015).
- [10] S. Diehl, A. Tomadin, A. Micheli, R. Fazio, and P. Zoller, *Nat. Phys.* **4**, 878 (2008); *Phys. Rev. Lett.* **105**, 015702 (2010); F. Verstraete, M. M. Wolf, and J. I. Cirac, *Nat. Phys.* **5**, 633 (2009); T. E. Lee, S. Gopalakrishnan, and M. D. Lukin, *Phys. Rev. Lett.* **110**, 257204 (2013); J. Jin, A. Biella, O. Viyuela, L. Mazza, J. Keeling, R. Fazio, and D. Rossini, *Phys. Rev. X* **6**, 031011 (2016).
- [11] E. G. D. Torre, E. Demler, T. Giamarchi, and E. Altman, *Phys. Rev. B* **85**, 184302 (2012).
- [12] J. Eisert and T. Prosen, [arXiv:1012.5013](https://arxiv.org/abs/1012.5013); M. Hönig, M. Moos, and M. Fleischhauer, *Phys. Rev. A* **86**, 013606 (2012).
- [13] B. Horstmann, J. I. Cirac, and G. Giedke, *Phys. Rev. A* **87**, 012108 (2013); M. Foss-Feig, J. T. Young, V. V. Albert, A. V. Gorshkov, and M. F. Maghrebi, *Phys. Rev. Lett.* **119**, 190402 (2017).
- [14] R. Bonifacio and L. A. Lugiato, *Phys. Rev. A* **18**, 1129 (1978); G. P. Agrawal and H. J. Carmichael, *ibid.* **19**, 2074 (1979).
- [15] R. Bonifacio and L. A. Lugiato, *Phys. Rev. Lett.* **40**, 1023 (1978); P. D. Drummond and D. F. Walls, *J. Phys. A* **13**, 725 (1980); S. R. K. Rodriguez, W. Casteels, F. Storme, N. Carlon Zambon, I. Sagnes, L. Le Gratiet, E. Galopin, A. Lemaître, A. Amo, C. Ciuti, and J. Bloch, *Phys. Rev. Lett.* **118**, 247402 (2017).
- [16] M. Foss-Feig, P. Niroula, J. T. Young, M. Hafezi, A. V. Gorshkov, R. M. Wilson, and M. F. Maghrebi, *Phys. Rev. A* **95**, 043826 (2017).
- [17] A. Dombi, A. Vukics, and P. Domokos, *J. Phys. B* **46**, 224010 (2013); J. J. Mendoza-Arenas, S. R. Clark, S. Felicetti, G. Romero, E. Solano, D. G. Angelakis, and D. Jaksch, *Phys. Rev. A* **93**, 023821 (2016); R. M. Wilson, K. W. Mahmud, A. Hu, A. V. Gorshkov, M. Hafezi, and M. Foss-Feig, *ibid.* **94**, 033801 (2016); W. Casteels, R. Fazio, and C. Ciuti, *ibid.* **95**, 012128 (2017).
- [18] R. Livi, R. Franzosi, and G.-L. Oppo, *Phys. Rev. Lett.* **97**, 060401 (2006); P. P. Orth, I. Stanic, and K. Le Hur, *Phys. Rev. A* **77**, 051601(R) (2008); T. Ramos, H. Pichler, A. J. Daley, and P. Zoller, *Phys. Rev. Lett.* **113**, 237203 (2014).
- [19] H.-P. Breuer and F. Petruccione, *The Theory of Open Quantum Systems* (Oxford University Press, Oxford, 2007).
- [20] P. Hedvall and J. Larson, [arXiv:1712.01560](https://arxiv.org/abs/1712.01560).
- [21] H. Spohn, *Lett. Math. Phys.* **2**, 33 (1977); A. Frigerio, *Commun. Math. Phys.* **63**, 269 (1978); F. Fagnola and R. Rebolledo, *J. Math. Phys.* **42**, 1296 (2001); **43**, 1074 (2002); B. Baumgartner and H. Narnhofer, *J. Phys. A* **41**, 395303 (2008); D. Nigro, [arXiv:1803.06279](https://arxiv.org/abs/1803.06279).
- [22] S. Schneider and G. J. Milburn, *Phys. Rev. A* **65**, 042107 (2002).
- [23] C. Gardiner and P. Zoller, *The Quantum World of Ultra-Cold Atoms and Light, Book 1, Foundations and Quantum Optics* (Imperial College Press, London, 2014).
- [24] M. P. Baden, K. J. Arnold, A. L. Grimsmo, S. Parkins, and M. D. Barrett, *Phys. Rev. Lett.* **113**, 020408 (2014).
- [25] R. Botet and R. Jullien, *Phys. Rev. B* **28**, 3955 (1983).
- [26] D. F. Walls, P. D. Drummond, S. S. Hassan, and H. J. Carmichael, *Prog. Theor. Phys.* **64**, 307 (1978).
- [27] P. D. Drummond and H. J. Carmichael, *Opt. Commun.* **27**, 160 (1978); P. D. Drummond, *Phys. Rev. A* **22**, 1179 (1980).
- [28] R. R. Puri and S. V. Lawande, *Phys. Lett. A* **72**, 200 (1979); S. V. Lawande, R. R. Puri, and S. S. Hassan, *J. Phys. B* **14**, 4171 (1981).
- [29] J. Larson and E. K. Irish, *J. Phys. A* **50**, 14002 (2017).
- [30] S. H. Strogatz, *Nonlinear Dynamics and Chaos* (Addison Wesley, Reading, MA, 1994).
- [31] M. A. Nielsen and I. L. Chuang, *Quantum Computation and Quantum Information* (Cambridge University Press, Cambridge, 2011).
- [32] W.-L. You, Y.-W. Li, and S.-J. Gu, *Phys. Rev. E* **76**, 022101 (2007); A. F. Albuquerque, F. Alet, C. Sire, and S. Capponi, *Phys. Rev. B* **81**, 064418 (2010).
- [33] T. J. Osborne and M. A. Nielsen, *Phys. Rev. A* **66**, 032110 (2002); A. Osterloh, L. Amico, G. Falci, and R. Fazio, *Nature (London)* **416**, 608 (2002).
- [34] J. Vidal and S. Dusuel, *Europhys. Lett.* **74**, 817 (2006).
- [35] K. Zyczkowski, P. Horodecki, A. Sanpera, and M. Lewenstein, *Phys. Rev. A* **58**, 883 (1998).

- [36] X. Wang and K. Mølmer, *Eur. Phys. J. D* **18**, 385 (2002).
- [37] V. Coffman, J. Kundu, and W. K. Wootters, *Phys. Rev. A* **61**, 052306 (2000).
- [38] A. Sørensen, L.-M. Duan, J. I. Cirac, and P. Zoller, *Nature (London)* **409**, 63 (2001).
- [39] B. M. Terhal, *Phys. Lett. A* **271**, 319 (2000).
- [40] S. Morrison and A. S. Parkins, *J. Phys. B: At. Mol. Opt.* **41**, 195502 (2008).
- [41] V. V. Albert and L. Jiang, *Phys. Rev. A* **89**, 022118 (2014); V. V. Albert, B. Bradlyn, M. Fraas, and L. Jiang, *Phys. Rev. X* **6**, 041031 (2016).
- [42] C. Joshi, J. Larson, and T. P. Spiller, *Phys. Rev. A* **93**, 043818 (2016).
- [43] R. Gilmore, C. Bowden, and L. Narducci, *Phys. Rev. A* **12**, 1019 (1975).
- [44] J. M. Radcliffe, *J. Phys. A* **4**, 313 (1971); F. T. Arecchi, E. Courtens, R. Gilmore, and H. Thomas, *Phys. Rev. A* **6**, 2211 (1972).
- [45] C. Emary and T. Brandes, *Phys. Rev. E* **67**, 066203 (2003).
- [46] As we have applied the RWA, in a strict sense the comparison should be to the Tavis-Cummings model and not the Dicke model, but regardless if the RWA has been employed or not does not change the argument.
- [47] B. Nienhuis, A. N. Berker, E. K. Riedel, and M. Schick, *Phys. Rev. Lett.* **43**, 737 (1979); E. Domany, M. Schick, and R. H. Swendsen, *ibid.* **52**, 1535 (1984).
- [48] R. Gilmore and C. M. Bowden, *J. Math. Phys.* **17**, 1617 (1976); R. Gilmore and L. M. Narducci, *Phys. Rev. A* **17**, 1747 (1978); E. M. Kessler, G. Giedke, A. Imamoglu, S. F. Yelin, M. D. Lukin, and J. I. Cirac, *ibid.* **86**, 012116 (2012).
- [49] J. Larson, *Europhys. Lett.* **90**, 54001 (2010).
- [50] T. E. Lee, C.-K. Chan, and S. F. Yelin, *Phys. Rev. A* **90**, 052109 (2014).
- [51] H. Wilming, M. J. Kastoryano, A. H. Werner, and J. Eisert, *J. Math. Phys.* **58**, 033302 (2017).
- [52] H. Hinrichsen, *Adv. Phys.* **49**, 815 (2000).
- [53] K. Baumann, C. Guerlin, F. Brennecke, and T. Esslinger, *Nature (London)* **464**, 1301 (2010); F. Brennecke, R. Mottl, K. Baumann, R. Landig, T. Donner, and T. Esslinger, *Proc. Natl. Acad. Sci. USA* **110**, 11763 (2013).
- [54] Z. Zhiqiang, C. H. Lee, R. Kumar, K. J. Arnold, S. J. Masson, A. S. Parkins, and M. D. Barrett, [arXiv:1612.06534](https://arxiv.org/abs/1612.06534).
- [55] S. Haroche and J.-M. Raimond, *Exploring the Quantum: Atoms, Cavities, and Photons* (Oxford University Press, Oxford, 2006).